Title: Nuclear quantum memory for hard X-ray photons

Authors: Sven Velten[1,2,*], Lars Bocklage[1,2], Xiwen Zhang[3], Kai Schlage[1], Anjali Panchwanee[1], Sakshath Sadashivaiah[4,5], Ilya Sergeev[1], Olaf Leupold[1], Aleksandr I. Chumakov[6], Olga Kocharovskaya[3], Ralf Röhlsberger[1,2,4,5,7]

Affiliations:

[1]Deutsches Elektronen-Synchrotron DESY, Notkestr. 85, 22607 Hamburg, Germany.

[2]The Hamburg Centre for Ultrafast Imaging CUI, 22761 Hamburg, Germany.

[3]Department of Physics and Astronomy and Institute for Quantum Science and Engineering, Texas A&M University, College Station, Texas 77843, USA.

[4]Helmholtz-Institut Jena, 07743 Jena, Germany.

[5]GSI Helmholtzzentrum für Schwerionenforschung GmbH, 64291 Darmstadt, Germany.

[6]ESRF - The European Synchrotron, CS40220, 38043 Grenoble Cedex 9, France.

[7]Friedrich-Schiller Universität Jena, 07743 Jena, Germany.

*Corresponding author. Email: sven.velten@desy.de

Abstract: Quantum memories are basic elements in complex quantum computing and communication networks for reliably storing and retrieving quantum information. Several protocols for quantum memories have been established but are limited to optical photons thus far. Here, we demonstrate a quantum memory for hard X-ray photons by employing a set of moving resonant nuclear ^{57}Fe absorbers. The setup enables us to control the photon propagation at a high level of accuracy and fidelity. Our protocol is based on the formation of a comb structure in the nuclear absorption spectrum using the Doppler effect. Such a tunable, robust, and highly flexible system offers a promising platform for a compact solid-state room temperature quantum memory in the hard X-ray range.

One-Sentence Summary: Doppler shifted nuclear resonant absorbers form a nuclear frequency comb as a quantum memory for hard X-ray photons.

Main Text:

Photons are fast and robust carriers of quantum information encoded in various degrees of freedom, including photon number, polarization, and waveform. But their fast propagating nature renders storage of quantum information challenging, which is instrumental not only for synchronization processes in quantum communication networks but also for the realization of quantum repeaters (*1–4*). Thus, there is a quest for quantum interfaces that enable to map photonic quantum bits (or qubits) to quantum excitations in a "slower" medium, such as atoms, molecules, rare-earth ions in crystals or color centers in diamond (*1*, *4–8*). In the visible wavelength regime, several mapping protocols have been developed which can store and retrieve single photonic qubits – so called quantum memories (*1*, *8*).

The step to shorter wavelength regimes, however, has not been achieved thus far, despite its benefits. Employing X-rays would allow to develop more compact and flexible quantum memory protocols due to X-rays being potentially focusable down to the angstrom scale, about four orders of magnitude shorter than wavelengths of visible photons, and higher penetration depths in many materials. To date, hard X-ray quantum memories have only been discussed theoretically (*9*, *10*). As quantum interface, nuclear resonances are potential candidates, especially the prominent 14.4 keV nuclear resonance of ^{57}Fe which was used to establish many quantum optical phenomena in the X-ray regime [see (*11*) and references therein]. Here, the photon-nuclei interaction benefits from high nuclear densities in solids (~ 10^{28} m^{-3}) and from a resonant cross-section being 400 times higher than the electronic scattering cross-section at this energy, resulting in high optical thicknesses even in physically thin absorbers. In addition, an excellent temporal coherence is achieved due to the narrow transition linewidth being more than twelve orders of magnitude smaller than the transition energy, even at room temperature. This is an important prerequisite for quantum memories since coherence must be maintained during the storage process. The outstanding coherence properties of nuclear resonances allow to temporally control the excited nuclear quantum state, as demonstrated by tuning the magnetic hyperfine interaction via magnon excitations (*12*) or via fast reversal or rotation of the nuclear magnetization (*9*, *13–15*), as well as by induced phase shifts via sudden movements of the resonant absorber (*16–19*), fast vibrating absorbers (*20–25*), thin film cavities (*26–30*) or motion induced Doppler shifts.

It is the latter approach, which was exploited in a recent proposal by X. Zhang *et al.* to form a quantum memory for hard X-ray photons using a set of moving resonant nuclear ^{57}Fe absorbers (*10*). With the small transition linewidths and the typical high transition energies E_0, a sizeable Doppler shift $\Delta E = E_0 v/c$, c being the speed of light, is achieved at comparatively small velocities v (a velocity of 0.1 mm/s readily shifts the ^{57}Fe transition by its natural linewidth). The proposed quantum memory concept is based on moving multiple resonant absorbers with different, but equidistantly spaced velocities to form a Doppler frequency comb in the nuclear absorption structure. When an incident resonant photon as a flying qubit is absorbed in such a frequency comb, its quantum information is stored in the nuclear excitation, and a photon carrying the same quantum information is re-emitted with a high probability at certain moments in time T_k ($k = 1,2,3,\ldots$), which are determined by the velocity spacing Δv between neighboring absorbers (*10*),

$$T_k = k \frac{hc}{E_0 \Delta v}, \qquad (1)$$

where h is the Planck constant. Photons emitted at these moments are referred to as "echoes". With the frequency comb parameters (bandwidth, teeth width, number of teeth) tuned correctly, an efficient and faithful quantum memory can be constructed, similar to atomic frequency combs in the optical regime (*31–33*). However, while atomic frequency combs are prepared by spectral hole burning within the broad inhomogeneous absorption linewidth by strong optical pulses which cannot be applied to nuclear systems, the nuclear frequency comb preparation is conceptually much simpler and straightforward. This promises to yield much sharper frequency combs that are ideally suited for quantum information storage.

Motivated by extending the quantum memory concept to the hard X-ray regime, we experimentally implement robust ^{57}Fe nuclear frequency combs with up to seven teeth and demonstrate its capacity to store and retrieve X-ray photons absorbed from a synchrotron X-ray pulse, as well as the single photon wave packet emitted by a thin film X-ray cavity which was spectrally designed to match the frequency comb's bandwidth. The latter approach showcases that quantum information is efficiently preserved, and therefore fulfilling the requirements of a quantum memory.

Coherent resonant scattering from a nuclear frequency comb

The setup contains seven single-line isotopically enriched stainless-steel foils ($^{57}Fe_{0.55}Cr_{0.25}Ni_{0.2}$) in a row with six of them mounted on Doppler velocity transducers, as sketched in Fig. 1A. The transducers are controlled by drive units synchronized with one sinusoidal master signal, such that the foils' motions follow the same sinusoidal pattern but with different maximum velocities. The maximum velocities are set equidistantly with a spacing of 10 mm/s, resulting in velocity profiles for each foil as shown in Fig. 1B. With the foil velocities following the master signal, the velocity spacings, and thus the Doppler shift between neighboring foils keep changing but remain always equidistant. For example, at maximum velocities, the Doppler shifted foils form a frequency comb in the combined absorption spectrum with a velocity spacing of 10 mm/s (= 480 neV), as depicted in Fig. 1C.

The experiments were conducted at the High-Resolution Dynamics Beamline P01 at PETRA III (DESY, Hamburg, Germany) (*34*) and at the Nuclear Resonance Beamline ID18 at ESRF (Grenoble, France) (*35*). In the experiments, the temporally short (< 100 ps) and spectrally broad (~0.5 meV or ~10,000 mm/s) synchrotron X-ray pulse creates a collectively excited nuclear state across all stainless-steel foils, known as a nuclear exciton [see (*36*, *37*) and references therein]. Subsequently, the decay of this collective excitation is modified by interferences between all possible Doppler shifted decay channels, resulting in temporal quantum beats. Despite the brightness of modern synchrotron radiation, the average number of photons per pulse within the spectral range of the frequency comb is about 0.01. Therefore, the collective excitation almost never carries more than one photon. The resulting single photon decay is detected by a set of four stacked avalanche photon diodes as a function of arrival time relative to the X-ray pulse, whereby the X-ray pulse separation (192 ns at PETRA III; 176 ns at ESRF) exceeds the natural lifetime (141 ns for ^{57}Fe). Collecting many of these single photon decay events results in a histogram related to the time dependent photon emission probability of the nuclear exciton, or synonymously, to the intensity of the emitted single photon wave packet (*24*). Besides the arrival time, the instantaneous velocity spacing of the concomitant frequency comb is also recorded, rendering the histogram two-dimensional. With the foils' velocity variations happening on timescales much slower (milliseconds^{-1}) than the nuclear decay rate (nanoseconds^{-1}), the velocities are virtually constant over the nuclear lifetime, resulting in a static frequency comb during each single photon scattering process.

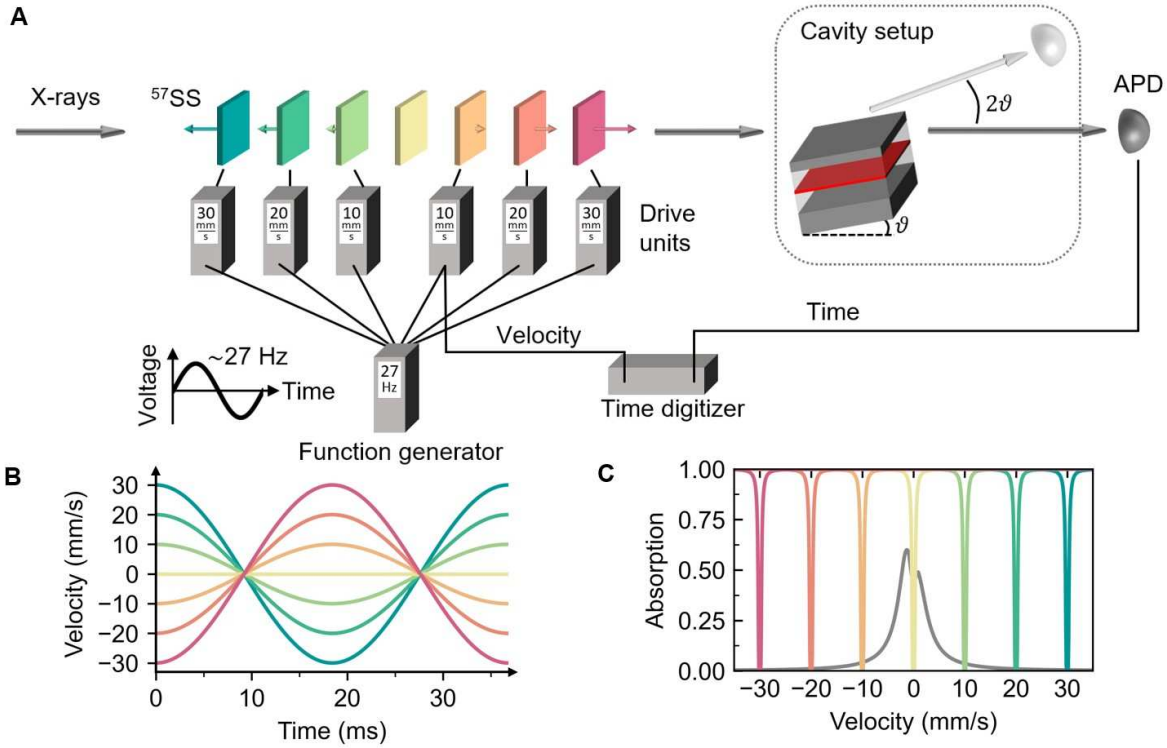

Fig. 1. Experimental setup. (**A**) Six isotopically enriched 3.2 μm thick ^{57}Fe stainless steel foils ($^{57}Fe_{0.55}Cr_{0.25}Ni_{0.2}$ %wt.; ^{57}SS) are mounted on six Mössbauer transducers (not shown), each individually driven by a drive unit. A seventh ^{57}SS foil is kept at rest. Each drive unit amplifies the AC voltage generated by a single function generator differently, such that the foils move with maximum velocities of 30 mm/s, 20 mm/s, 10 mm/s, -10 mm/s, -20 mm/s and -30 mm/s. The negative sign indicates a 180° motional phase shift realized by flipping the respective transducer. The nuclear resonance is excited by X-ray pulses from the synchrotron. The photon detection time and the instantaneous velocity of one Mössbauer transducer are simultaneously recorded using a multiple-event time digitizer. The cavity is mounted optionally (sequence of cavity and foils is irrelevant, see Supplemental Materials). (**B**) Velocity profile of each foil, following the 27 Hz AC driving voltage. (**C**) Combined nuclear resonant absorption spectrum of the foils driven at maximum velocity, resulting in a frequency comb with a velocity spacing of 10 mm/s (= 480 neV). The spectrum of the single photon wave packet emitted by the cavity is plotted in the background (arb. u.).

The accumulated histogram for the frequency comb setup is shown in Fig. 2A, from which four columns corresponding to four different velocity spacings between the foils are selected in Fig. 2B. The histograms in Fig. 2B reflect the unnormalized single photon emission probability of the nuclear exciton for different velocity spacings, and clearly show equidistantly repeating time instants of enhanced photon emission – the echoes from the frequency comb. From Eq. (1), the echo period increases from $\Delta T = 8.6$ ns to 34 ns when the velocity spacing reduces from $\Delta v = 10$ mm/s to 2.5 mm/s, agreeing well with the experimental observations. In the meantime, the full width at half maximum of the echoes decreases from 4.4(3) ns at 2.5 mm/s to 1.2(1) ns at 10 mm/s, showing an inverse proportionality to the total bandwidth of the frequency comb. The observed patterns closely resemble interference patterns obtained from spatial diffraction gratings (see Supplementary Materials).

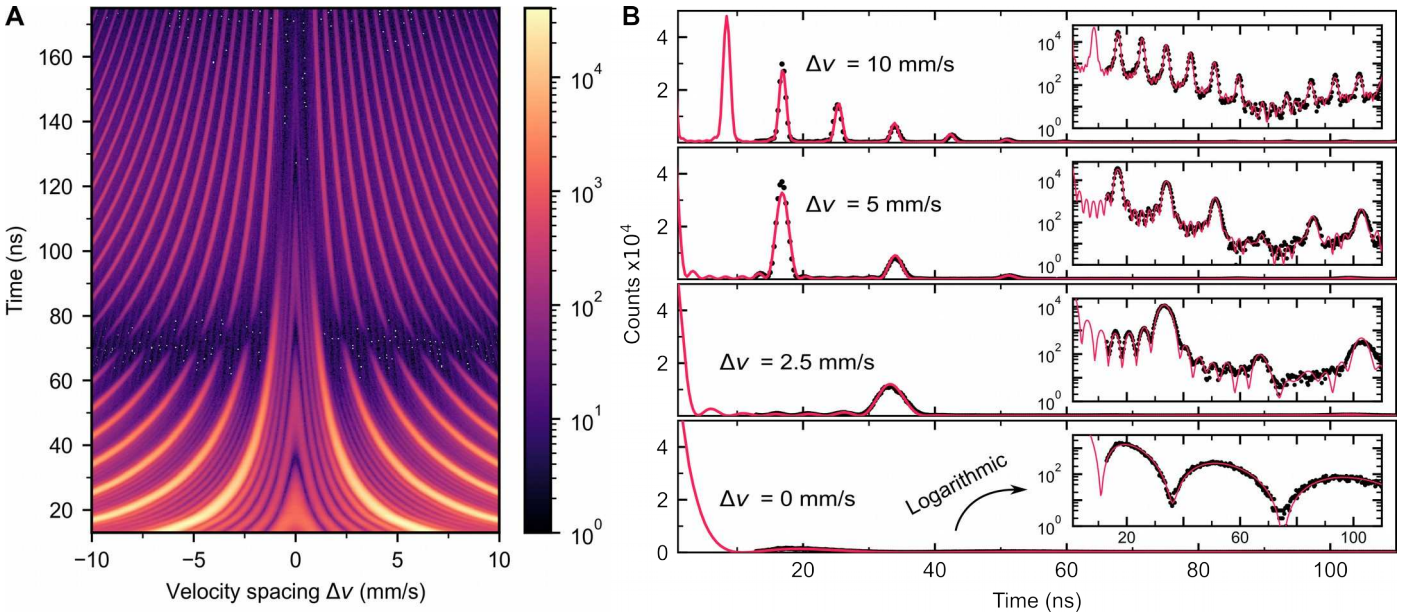

Fig. 2. **Single photon decay from nuclear frequency comb.** (**A**) Time-velocity histogram of the single photon decay of a nuclear exciton spectrally prepared in a frequency comb consisting of seven teeth, equally spaced over a Doppler detuning range extending from -10 mm/s to 10 mm/s (≈ 480 neV). The color map displays the number of detected photons on a logarithmic scale. (**B**) Decay histogram for four selected velocity spacings from (A) in linear and logarithmic scales. The patterns are simulated using the software package *Nexus* (red).

The drastic reshaping of the emission probability due to the frequency comb is best seen in comparison with the case when no foil is moving ($\Delta v = 0$ mm/s). In this case, the emission probability follows the superradiant decay from a 22 μm thick stainless steel foil (7×3.2 μm) with dynamical beats typical for optically thick absorbers due to multiscattering (*10*, *38*). But when the foils are moving and forming a frequency comb, the emission probability is completely reshaped into a repetitive structure, where the emission is drastically enhanced at the echoes and decreased in between.

The experimental result is supported by simulations carried out using the software package *Nexus* (*39*), which calculates the total (resonant and non-resonant) forward scattering intensity of the experiment in frequency domain (*40*). Both agree with our time-domain simulations based on Maxwell-Bloch equations. With material and hyperfine parameters of each foil being determined by previous characterization (see Supplementary Materials), the simulations shown in Fig. 2B match the measurements very well, which demonstrates the accurateness of our setup. Also, the predicted quantum beats in between two echoes, arising due to partial constructive interferences between the Doppler shifted transitions, are experimentally well resolved.

The results confirm a well-functioning nuclear frequency comb. With this, we can now demonstrate the quantum memory performance of the nuclear frequency comb. For that purpose, we placed a thin film X-ray cavity in the beam path, which emits a single photon wave packet with a spectrum matching the frequency comb bandwidth. Now, the cavity-frequency comb setup should emit this wave packet at each echo, rendering the cavity response retrievable far beyond its normal response time.

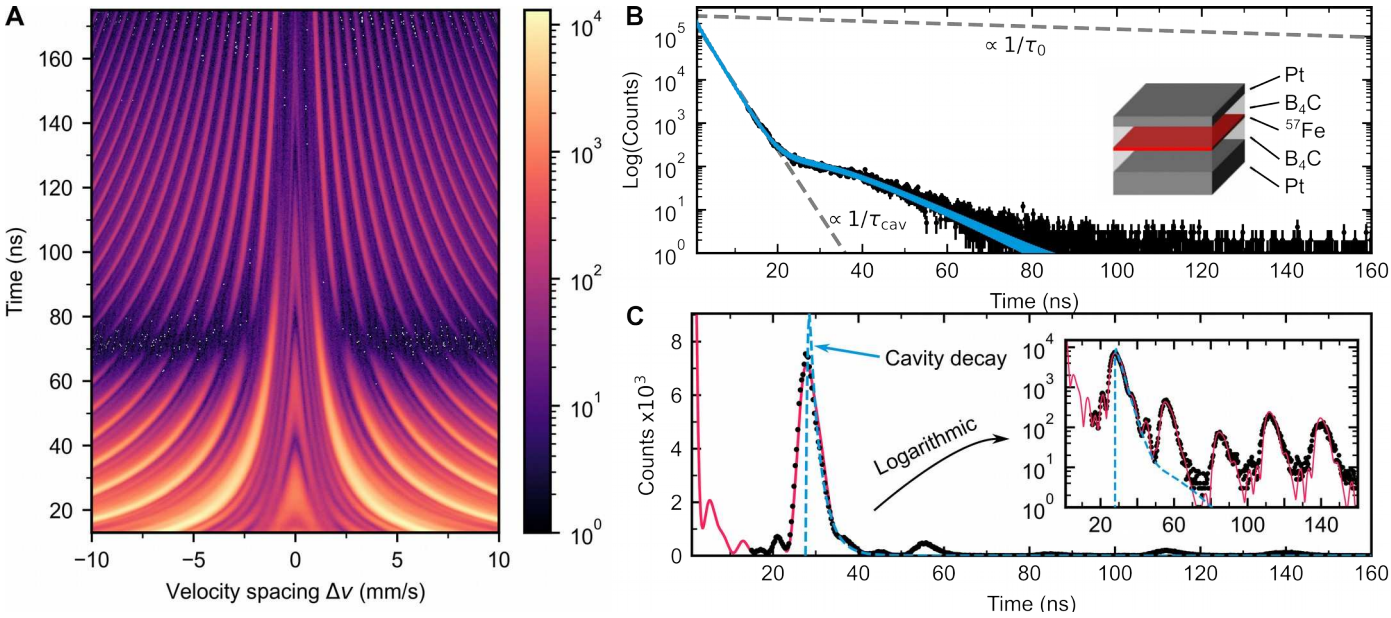

Fig. 3. Quantum memory data. (**A**) Time-velocity histogram of the same frequency comb as shown in Fig. 2, in combination with a thin film cavity excited in its first waveguide mode at an incident angle of 0.1505°. (**B**) Measured (black) and fitted (blue) decay histograms of the thin film cavity alone, excited in its first waveguide mode. The initial strong speed-up in the cavity decay corresponds to an exponential decay [$\propto \exp$ ¿), with τ_{cav}=¿ 2.9(2) ns], in comparison to the natural exponential decay of the excited ^{57}Fe state with τ_0 = 141 ns. The inset shows the layer structure of the cavity consisting of: Pt (2.3 nm)/ B_4C (13.1 nm)/ ^{57}Fe (1.1 nm)/ B_4C (12.8 nm)/ Pt (15.0 nm)/ Al_2O_3 (substrate; not shown). (**C**) Extracted decay histogram from (A) at the velocity spacing of 3.1 mm/s (≈ 240 neV) with measurement (black) and fit (red) in linear and logarithmic scales. The derived cavity decay from (B) is overlaid (blue) at the first echo, showing the matching decay of the echo and the cavity intensities. More decay histograms for different velocity spacings are depicted in the Supplementary Materials.

Quantum storage of a cavity photon

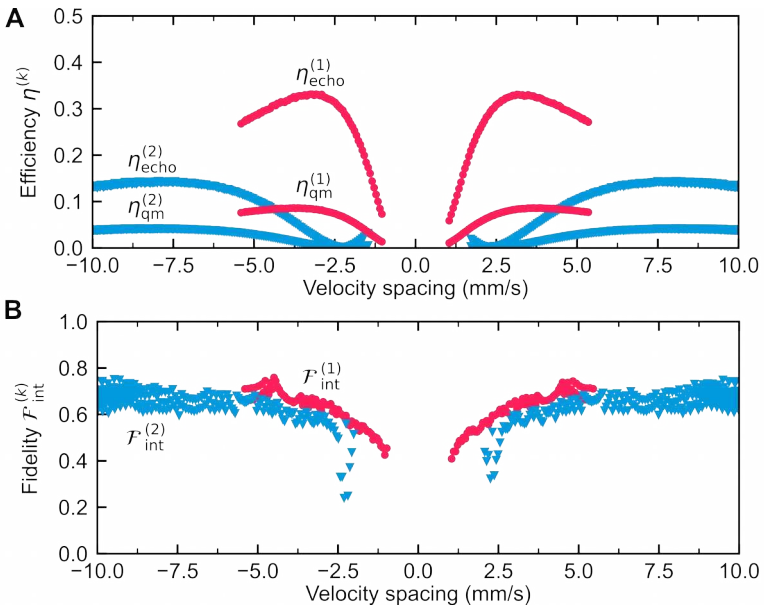

Fig. 4. Quantum memory parameters. Derived echo efficiency $\eta^{(k)}_{echo}$, quantum memory efficiency $\eta^{(k)}_{qm}$ (**A**) and intensity fidelity $F_{\int ¿^{(k)} ¿}$ (**B**) for the k-th echo [$k=1$ (red) or $k=2$ (blue)] of the cavity-frequency comb setup as a function of the velocity spacing. For echoes appearing early, < 13 ns (detection dead time), or late, at > 100 ns (low intensity), no meaningful values of efficiency and fidelity could be derived.

We combined the frequency comb setup with a thin film X-ray cavity which is aligned in a grazing incidence configuration along the X-ray beam path downstream of the seven foils as depicted in Fig. 1A. The sequence of the cavity and foils is irrelevant in our case due to the scattering matrices being diagonal (see Supplementary Materials). The cavity consists of a stack of nanometer thin films (see sketch in Fig. 3B, details in Supplementary Materials). At a particular incidence angle, the X-ray field couples into the first order waveguide mode and peaks in the center of the cavity, where an isotopically enriched ^{57}Fe layer is located. This enhances the photon-nuclei interaction, resulting in a superradiant collective nuclear state (*27*). The measured intensity of the subsequently emitted single photon wave packet, depicted in Fig. 3B, shows accordingly an accelerated decay: in the first 20 ns the decay follows an exponential law with a drastically reduced lifetime of $\tau_{cav}=¿$ 2.9(2) ns. This corresponds to a transition linewidth being 47(3) times broader than the natural linewidth, and thus, fitting within the scanned bandwidth range of the frequency comb, see Fig. 1C. The fast decay is slowed down after 20 ns when a quantum beat sets in, caused by a residual quadrupole splitting of the nuclear levels of 29 neV. This splitting is much smaller than the superradiant broadening and does not affect the overall spectrum of the emitted wave packet.

The collected histogram of the combined cavity-frequency comb setup is shown in Fig. 3A. Again, enhanced emission at the echoes is clearly visible, but the echo shape becomes temporally asymmetric. The photon emission for a velocity spacing of 3.1 mm/s, shown in Fig. 3C, fully confirms the asymmetric shape: the rising edges of the echoes are very sharp, while the falling edges follow an exponential decay (linear slope in the logarithmic representation). The echo shape exactly reflects the photon wave packet shape emitted by the cavity alone. It is both visible in the experimental data and in the simulations. In other words, the cavity response is stored and

retrieved at predefined times which largely exceed the cavity lifetime τ_{cav}. It demonstrates the functionality of the nuclear frequency comb as a quantum memory.

Our quantum memory's performance can be quantified by the echo efficiency, i.e. the number of emitted photons within an echo duration relative to the total number of coherently forward scattered photons, and by the fidelity of the storage process, i.e. how well the temporal shape of the wave packet emitted by the cavity is preserved (see calculation details in Supplementary Materials). With the simulations matching the measurements very well, they can be justifiably used to extrapolate the temporal quantum patterns to time zero. Experimentally it is not accessible due to a strong non-resonant part of the synchrotron pulse perturbing the detection scheme at early times. The extrapolation enables the evaluation of the total number of emitted photons, therefore of the echo efficiency and fidelity. Due to the lack of phase information in our measurements, only an intensity-based fidelity is calculable. However, for static frequency combs, the phases of the echoes are predicted to be well preserved, rendering the intensity fidelity a good approximation for the complex amplitude-based fidelity (*10*, *41*).

The calculated echo efficiency as a function of the velocity spacing is shown in Fig. 4A. The echo efficiency peaks for the first echo at 33(1)% for a velocity of 3.1 mm/s, and decreases for low velocity spacings quickly, while for high velocity spacings more moderately. This is mainly caused by two effects: firstly, by the finite lifetime of the nuclear exciton, which is related to the spectral width of a single comb tooth (relevant for small velocity spacings, where echoes appear late), and secondly, by the decay into higher order echoes (relevant for high velocity spacings, where the echo periods are small).

Note that the calculated echo efficiency does not account for photon losses due to non-resonant electronic charge interactions and incoherent nuclear scattering, which result in a total energy loss of 74% for a velocity spacing of 3.1 mm/s (see Supplementary Materials). A quantum memory efficiency accounting for these losses is depicted in Fig. 4A. For 3.1 mm/s, η_{qm} is 8% for the first echo, a value comparable to optical fixed-delays atomic frequency combs (*42*–*45*). This can be compared to the analytical quantum memory efficiency X. Zhang *et al.* derived for the storage of a Gaussian wave packet (*10*). For the same experimental parameters and including electronic interactions, the expression yields 13.1%, with a theoretical upper limit of 18.4% (54% if electronic interactions are neglected) imposed by multiscattering (*10*). Despite the different shapes of the stored wave packets, the measured efficiency is close to the theoretical predictions, and not far from the upper limit. An efficiency increase could be accomplished by increasing the optical thickness of the foils (*10*). Furthermore, higher efficiencies could also be realized by more sophisticated nuclear quantum memory protocols, which requires the use of fast piezoelectric materials (*10*).

The calculated fidelity is shown in Fig. 4B. It monotonically increases with the velocity spacing, but saturates for higher velocities at 67(4)%. At very low velocity spacings ($\lesssim$ 1.5 mm/s), the comb bandwidth is too narrow to maintain the temporal waveform of the cavity decay. Moreover, the echo shape can be altered by the single-foil dynamical beat node at around 70 ns as they temporally coincide at $\sim$1.25 mm/s and $\sim$2.5 mm/s for the first and the second echoes, respectively. For large velocity spacings, the number of measurement points becomes insufficient for a precise calculation of the fidelity due to the reduced echo period, noticeable by the increased spread of fidelity values in Fig. 4B.

The fidelity of the photon emission does not quite reach values necessary for faithful quantum memory operation (typically >90%). This is largely due to the step-like rising edge in the cavity

decay at time zero. If this edge is neglected, the derived fidelity reaches 97(1)%. Such a step-like edge cannot be well reproduced by the frequency comb because of its limited bandwidth. The comb bandwidth can be increased by adding more foils while keeping the same velocity spacing (a comb with eleven teeth would result in a fidelity of 75%). In addition, an "imperfect source", i.e. non-resonantly scattered cavity photons, also contributes to the fidelity degradation (see Supplementary Materials). The fidelity can be significantly increased for photons with a smooth leading edge which can be produced from the Mössbauer synchrotron sources after passing a vibrated resonant absorber (*24*).

The fidelity also depends on the actual photon degree of freedom to be stored. The fidelity in Fig. 4B is defined based on recovering the cavity's photon waveform, for which a small shape variation may already lead to a lower fidelity. If, instead, a polarization encoding quantum memory is of interest (*46*, *47*), the fidelity is practically 100% since a nuclear scattering process from a single line does not alter the polarization state.

In total, for the given optical thicknesses of the foils and cavity decay properties, a velocity spacing of 3.1 mm/s appears to be optimal for storing and recovering the wave packet emitted by the cavity with good efficiency and decent fidelity.

Conclusion

Overall, our nuclear frequency comb demonstrated the storage of quantum information in the hard X-ray regime, constituting a quantum memory with reasonable efficiency and fidelity. Our quantum memory concept is not restricted to the ^{57}Fe resonance, but can be applied to all resonances, which are tunable via temporally well controlled Doppler motions. This is possible for all Mössbauer nuclear resonances, e.g. the 12.4 keV transition of ^{45}Sc with its long lifetime of 0.46 s which would greatly increase the quantum storage duration (*48*). The flexibility as well as the tunability of the Doppler frequency comb renders it a promising platform for quantum memory protocols to be integrated in future quantum computing frameworks for hard X-rays (*46*, *49*).

In further development of our quantum memory concept, the Doppler shifts can also be created by micro- or nanostructured piezoelectrical materials (*50*) that allow fast switching of the moving directions of the foils or enable a rapid stop-and-release motion on the nanosecond time scale, shorter than the lifetime of the excited nuclei. These motion patterns allow to increase the efficiency of the quantum memory and to alter the phase evolutions of the excited nuclei, which will result in a fast and versatile control of the echo emission (*10*).

References and Notes

1. A. I. Lvovsky, B. C. Sanders, W. Tittel, Optical quantum memory. *Nature Photon*. **3**, 706–714 (2009).

2. T. Chanelière, D. N. Matsukevich, S. D. Jenkins, S.-Y. Lan, T. a. B. Kennedy, A. Kuzmich, Storage and retrieval of single photons transmitted between remote quantum memories. *Nature*. **438**, 833–836 (2005).

3. J. L. O'Brien, A. Furusawa, J. Vučković, Photonic quantum technologies. *Nature Photon*. **3**, 687–695 (2009).

4. M. K. Bhaskar, R. Riedinger, B. Machielse, D. S. Levonian, C. T. Nguyen, E. N. Knall, H. Park, D. Englund, M. Lončar, D. D. Sukachev, M. D. Lukin, Experimental demonstration of memory-enhanced quantum communication. *Nature*. **580**, 60–64 (2020).

5. M. D. Lukin, Colloquium: Trapping and manipulating photon states in atomic ensembles. *Rev. Mod. Phys.* **75**, 457–472 (2003).

6. I. Novikova, R. l. Walsworth, Y. Xiao, Electromagnetically induced transparency-based slow and stored light in warm atoms. *Laser & Photonics Reviews*. **6**, 333–353 (2012).

7. D. Serrano, S. K. Kuppusamy, B. Heinrich, O. Fuhr, D. Hunger, M. Ruben, P. Goldner, Ultra-narrow optical linewidths in rare-earth molecular crystals. *Nature*. **603**, 241–246 (2022).

8. T. Chanelière, G. Hétet, N. Sangouard, "Chapter Two - Quantum Optical Memory Protocols in Atomic Ensembles" in *Advances In Atomic, Molecular, and Optical Physics*, E. Arimondo, L. F. DiMauro, S. F. Yelin, Eds. (Academic Press, 2018; https://www.sciencedirect.com/science/article/pii/S1049250X18300028), vol. 67, pp. 77–150.

9. W.-T. Liao, A. Pálffy, C. H. Keitel, Coherent Storage and Phase Modulation of Single Hard-X-Ray Photons Using Nuclear Excitons. *Phys. Rev. Lett.* **109**, 197403 (2012).

10. X. Zhang, W.-T. Liao, A. Kalachev, R. Shakhmuratov, M. Scully, O. Kocharovskaya, Nuclear Quantum Memory and Time Sequencing of a Single γ Photon. *Phys. Rev. Lett.* **123**, 250504 (2019).

11. R. Röhlsberger, J. Evers, S. Shwartz, "Quantum and Nonlinear Optics with Hard X-Rays" in *Synchrotron Light Sources and Free-Electron Lasers: Accelerator Physics, Instrumentation and Science Applications*, E. Jaeschke, S. Khan, J. R. Schneider, J. B. Hastings, Eds. (Springer International Publishing, Cham, 2014; https://doi.org/10.1007/978-3-319-04507-8_32-1), pp. 1–28.

12. L. Bocklage, J. Gollwitzer, C. Strohm, C. F. Adolff, K. Schlage, I. Sergeev, O. Leupold, H.-C. Wille, G. Meier, R. Röhlsberger, Coherent control of collective nuclear quantum states via transient magnons. *Science Advances*. **7**, eabc3991 (2021).

13. Yu. V. Shvyd'ko, T. Hertrich, J. Metge, O. Leupold, E. Gerdau, H. D. Rüter, Reversed time in Mössbauer time spectra. *Phys. Rev. B*. **52**, R711–R714 (1995).

14. Yu. V. Shvyd'ko, T. Hertrich, U. van Bürck, E. Gerdau, O. Leupold, J. Metge, H. D. Rüter, S. Schwendy, G. V. Smirnov, W. Potzel, P. Schindelmann, Storage of Nuclear Excitation Energy through Magnetic Switching. *Phys. Rev. Lett.* **77**, 3232–3235 (1996).

15. X. Kong, A. Pálffy, Stopping Narrow-Band X-Ray Pulses in Nuclear Media. *Phys. Rev. Lett.* **116**, 197402 (2016).

16. P. Helistö, I. Tittonen, M. Lippmaa, T. Katila, Gamma echo. *Phys. Rev. Lett.* **66**, 2037–2040 (1991).

17. K. P. Heeg, A. Kaldun, C. Strohm, P. Reiser, C. Ott, R. Subramanian, D. Lentrodt, J. Haber, H.-C. Wille, S. Goerttler, R. Rüffer, C. H. Keitel, R. Röhlsberger, T. Pfeifer, J. Evers, Spectral narrowing of x-ray pulses for precision spectroscopy with nuclear resonances. *Science*. **357**, 375–378 (2017).

18. K. P. Heeg, A. Kaldun, C. Strohm, C. Ott, R. Subramanian, D. Lentrodt, J. Haber, H.-C. Wille, S. Goerttler, R. Rüffer, C. H. Keitel, R. Röhlsberger, T. Pfeifer, J. Evers, Coherent X-ray–optical control of nuclear excitons. *Nature*. **590**, 401–404 (2021).

19. R. N. Shakhmuratov, F. Vagizov, O. Kocharovskaya, Single gamma-photon revival from sandwich absorbers. *Phys. Rev. A*. **87**, 013807 (2013).

20. F. Vagizov, V. Antonov, Y. V. Radeonychev, R. N. Shakhmuratov, O. Kocharovskaya, Coherent control of the waveforms of recoilless γ-ray photons. *Nature*. **508**, 80–83 (2014).

21. Y. V. Radeonychev, I. R. Khairulin, F. G. Vagizov, M. Scully, O. Kocharovskaya, Observation of Acoustically Induced Transparency for γ-Ray Photons. *Phys. Rev. Lett.* **124**, 163602 (2020).

22. R. N. Shakhmuratov, F. G. Vagizov, V. A. Antonov, Y. V. Radeonychev, M. O. Scully, O. Kocharovskaya, Transformation of a single-photon field into bunches of pulses. *Phys. Rev. A*. **92**, 023836 (2015).

23. I. R. Khairulin, Y. V. Radeonychev, O. Kocharovskaya, Slowing down x-ray photons in a vibrating recoilless resonant absorber. *Sci Rep*. **12**, 20270 (2022).

24. I. R. Khairulin, Y. V. Radeonychev, O. Kocharovskaya, Compression of the Synchrotron Mössbauer X-ray Photon Waveform in an Oscillating Resonant Absorber. *Photonics*. **9**, 829 (2022).

25. X. Zhang, A. A. Svidzinsky, Superradiant control of γ-ray propagation by vibrating nuclear arrays. *Phys. Rev. A*. **88**, 033854 (2013).

26. R. Röhlsberger, H.-C. Wille, K. Schlage, B. Sahoo, Electromagnetically induced transparency with resonant nuclei in a cavity. *Nature*. **482**, 199–203 (2012).

27. R. Röhlsberger, K. Schlage, B. Sahoo, S. Couet, R. Rüffer, Collective Lamb Shift in Single-Photon Superradiance. *Science*. **328**, 1248–1251 (2010).

28. J. Haber, X. Kong, C. Strohm, S. Willing, J. Gollwitzer, L. Bocklage, R. Rüffer, A. Pálffy, R. Röhlsberger, Rabi oscillations of X-ray radiation between two nuclear ensembles. *Nature Photon*. **11**, 720–725 (2017).

29. J. Haber, K. S. Schulze, K. Schlage, R. Loetzsch, L. Bocklage, T. Gurieva, H. Bernhardt, H.-C. Wille, R. Rüffer, I. Uschmann, G. G. Paulus, R. Röhlsberger, Collective strong coupling of X-rays and nuclei in a nuclear optical lattice. *Nature Photon*. **10**, 445–449 (2016).

30. K. P. Heeg, H.-C. Wille, K. Schlage, T. Guryeva, D. Schumacher, I. Uschmann, K. S. Schulze, B. Marx, T. Kämpfer, G. G. Paulus, R. Röhlsberger, J. Evers, Vacuum-Assisted Generation and Control of Atomic Coherences at X-Ray Energies. *Phys. Rev. Lett.* **111**, 073601 (2013).

31. M. Afzelius, C. Simon, H. de Riedmatten, N. Gisin, Multimode quantum memory based on atomic frequency combs. *Phys. Rev. A*. **79**, 052329 (2009).

32. D. Lago-Rivera, S. Grandi, J. V. Rakonjac, A. Seri, H. de Riedmatten, Telecom-heralded entanglement between multimode solid-state quantum memories. *Nature*. **594**, 37–40 (2021).

33. H. de Riedmatten, M. Afzelius, M. U. Staudt, C. Simon, N. Gisin, A solid-state light–matter interface at the single-photon level. *Nature*. **456**, 773–777 (2008).

34. H.-C. Wille, H. Franz, R. Röhlsberger, W. A. Caliebe, F.-U. Dill, Nuclear resonant scattering at PETRA III : Brillant opportunities for nano – and extreme condition science. *J. Phys.: Conf. Ser.* **217**, 012008 (2010).

35. R. Rüffer, A. I. Chumakov, Nuclear Resonance Beamline at ESRF. *Hyperfine Interact*. **97**, 589–604 (1996).

36. Yu. Kagan, Theory of coherent phenomena and fundamentals in nuclear resonant scattering. *Hyperfine Interactions*. **123**, 83–126 (1999).

37. J. P. Hannon, G. T. Trammell, Coherent γ-ray optics. *Hyperfine Interactions*. **123**, 127–274 (1999).

38. G. V. Smirnov, General properties of nuclear resonant scattering. *Hyperfine Interactions*. **123**, 31–77 (1999).

39. L. Bocklage, Nexus - Nuclear Elastic X-ray scattering Universal Software (2023), , doi:10.5281/zenodo.7716207.

40. W. Sturhahn, E. Gerdau, Evaluation of time-differential measurements of nuclear-resonance scattering of x rays. *Phys. Rev. B*. **49**, 9285–9294 (1994).

41. X. Zhang, Exact solution of gradient echo memory and analytical treatment of gradient frequency comb (2016), , doi:10.48550/arXiv.1602.05115.

42. M. F. Askarani, A. Das, J. H. Davidson, G. C. Amaral, N. Sinclair, J. A. Slater, S. Marzban, C. W. Thiel, R. L. Cone, D. Oblak, W. Tittel, Long-Lived Solid-State Optical Memory for High-Rate Quantum Repeaters. *Phys. Rev. Lett.* **127**, 220502 (2021).

43. P. Jobez, N. Timoney, C. Laplane, J. Etesse, A. Ferrier, P. Goldner, N. Gisin, M. Afzelius, Towards highly multimode optical quantum memory for quantum repeaters. *Phys. Rev. A*. **93**, 032327 (2016).

44. C. Clausen, I. Usmani, F. Bussières, N. Sangouard, M. Afzelius, H. de Riedmatten, N. Gisin, Quantum storage of photonic entanglement in a crystal. *Nature*. **469**, 508–511 (2011).

45. Z.-Q. Zhou, J. Wang, C.-F. Li, G.-C. Guo, Efficient spectral hole-burning and atomic frequency comb storage in Nd3+:YLiF4. *Sci Rep*. **3**, 2754 (2013).

46. J. Gunst, C. H. Keitel, A. Pálffy, Logical operations with single x-ray photons via dynamically-controlled nuclear resonances. *Sci Rep*. **6**, 25136 (2016).

47. A. Pálffy, C. H. Keitel, J. Evers, Single-Photon Entanglement in the keV Regime via Coherent Control of Nuclear Forward Scattering. *Phys. Rev. Lett.* **103**, 017401 (2009).

48. Yu. V. Shvyd'ko, R. Röhlsberger, O. Kocharovskaya, J. Evers, G. A. Geloni, Resonant X-ray excitation of the nuclear clock isomer 45Sc (in print). *Nature*.

49. J. Gunst, A. Pálffy, X-ray quantum-eraser setup for time-energy complementarity. *Phys. Rev. A.* **94**, 063849 (2016).

50. F. Wu, W. Cai, Y.-W. Yeh, S. Xu, N. Yao, Energy scavenging based on a single-crystal PMN-PT nanobelt. *Sci Rep*. **6**, 22513 (2016).

51. R. Röhlsberger, "Coherent Elastic Nuclear Resonant Scattering" in *Nuclear Condensed Matter Physics with Synchrotron Radiation: Basic Principles, Methodology and Applications*, R. Röhlsberger, Ed. (Springer, Berlin, Heidelberg, 2004; https://doi.org/10.1007/978-3-540-44699-6_4), *Springer Tracts in Modern Physics*, pp. 67–180.

52. Y.-H. Chen, M.-J. Lee, I.-C. Wang, S. Du, Y.-F. Chen, Y.-C. Chen, I. A. Yu, Coherent Optical Memory with High Storage Efficiency and Large Fractional Delay. *Phys. Rev. Lett.* **110**, 083601 (2013).

53. B. Sahoo, K. Schlage, J. Major, U. von Hörsten, W. Keune, H. Wende, R. Röhlsberger, Preparation and Characterization of Ultrathin Stainless Steel Films. *AIP Conference Proceedings*. **1347**, 57–60 (2011).

54. G. V. Smirnov, V. G. Kohn, Theory of nuclear resonant scattering of synchrotron radiation in the presence of diffusive motion of nuclei. *Phys. Rev. B*. **52**, 3356–3365 (1995).

55. B. Herkommer, J. Evers, Phase-sensitive nuclear target spectroscopy. *Phys. Rev. Res.* **2**, 023397 (2020).

Acknowledgments: We thank Dieter Lott for the access to X-ray reflection and diffraction instruments, Andrey Siemens for excellent technical support, Guido Meier for fruitful discussions and Georg Steinbrück, as well as Ingo Uschmann for the provision of Mössbauer spectroscopy equipment.

Funding:

S.V., L.B. and R.R. acknowledge funding from the Cluster of Excellence „CUI: Advanced Imaging of Matter“ of the Deutsche Forschungsgemeinschaft (DFG) – EXC 2056 – project ID 390715994. X.Z. and O.K. acknowledge support by the National Science Foundation (grant No. PHY-2012194 “Quantum Optics with Ultra-Narrow Gamma Resonances”).

Author contributions:

R.R. conceived the experiment,

R. R. and O. K. supervised the project,

R.R., L.B., S.V., I.S., A.C., and X.Z. developed the experimental methods,

L.B., S.V., and X.Z. developed software for theoretical simulations and data evaluation,

I.S., A.C., R.R., L.B., S.V., and O.L. provided experimental resources for the experimental setup,

S.V., L.B., X.Z., K.S., A.P., S.S., O.L., I.S., and R.R. performed the experiments,

S.V. and X.Z. evaluated and analyzed the data,

S. V. realized the visualization of data and calculations,

R. R. acquired funds for realization of the project,

S. V. wrote the first draft of the manuscript,

S.V., L.B., X.Z., R.R., and O.K. reviewed and edited all further versions of the manuscript with contributions from all authors,

S.V., L.B., K.S., S.S., O.L., I.S., A.C., and R.R. discussed and improved the manuscript.

Competing interests: Authors declare that they have no competing interests.

Data and materials availability: Data and code will be made publicly and immediately available at *Zenodo* after the review process is concluded.

Supplementary Materials

Materials and Methods

Supplementary Text

Figs. S1 to S5

Tables S1 to S3

References (*51–55*)